Published in final edited form as:

Proc IEEE Int Symp Biomed Imaging. 2019 April ; 2019: 422–425. doi:10.1109/ISBI.2019.8759379.

CHARTING DEVELOPMENT-BASED JOINT PARCELLATION MAPS OF HUMAN AND MACAQUE BRAINS DURING INFANCY

Jing Xia[1,2], **Fan Wang**[2], **Zhengwang Wu**[2], **Li Wang**[2], **Yaping Wang**[3], **Caiming Zhang**[1], **Weili Lin**[2], **Dinggang Shen**[2], **Gang Li**[2,*]

[1]Department of Computer Science and Technology, Shandong University, Shandong, China

[2]Department of Radiology and BRIC, University of North Carolina at Chapel Hill, NC 27599, USA

[3]School of Information Engineering, Zhengzhou University, Henan, China

Abstract

Comparative characterization of early brain development between human and macaque using neuroimaging data is crucial to understand the mechanisms of brain development and evolution. To this end, joint cortical parcellation maps of human and macaque infant brains with corresponding regions are highly desirable, since they provide basic cortical parcels for both region-based and network-based studies of two closely-related species. To address this issue, we propose to leverage developmental patterns of cortical properties of both human and macaque infants for creating joint parcellation maps with inter-species comparability. The motivation is that the developmental patterns of cortical properties indicate underlying rapid changes of microstructures, which determine the molecular and functional principles of the cortex. Thus, developmental patterns are well suitable for defining distinct cortical regions in both structures and functions. To comprehensively capture the similarities of developmental patterns of vertices on cortical surfaces, for each species, we first construct two complementary similarity matrices: a *low-order* matrix and a *high-order* matrix. Then, we *non-linearly* fuse these four matrices together as a single matrix in a *hierarchical* manner, thus capturing the common and complementary information of both human and macaque infants. Finally, based on the fused similarity matrix, we apply the spectral clustering to derive the joint parcellation maps. By applying our method to 210 longitudinal human infant MRI scans and 140 longitudinal macaque infant MRI scans, we generate the first biologically-meaningful joint parcellation maps of human and macaque infants.

Keywords

Macaque infants; joint parcellation

1. INTRODUCTION

Nonhuman primates, especially the macaque monkeys with close phylogenetic relationship to human, are a widely used animal model for human neuroscience studies [1]. Comparative characterization of early postnatal brain development [2, 3] between human and macaque

*Corresponding author: gang_li@med.unc.edu.

using neuroimaging data plays an important role in understanding the underlying mechanisms of brain development, evolution, and neurodevelopmental disorders [1, 4, 5]. In neuroimaging studies, cortical parcellation aims to partition the cerebral cortex into a series of regions/parcels, where each parcel has homogeneous territories that share similar microstructural or functional organization. Hence, a cortical parcellation map is an essential dimensionality reduction tool for region-based and network-based neuroimaging analyses. Accordingly, the joint parcellation maps of human and macaque infant brains can provide common cortical basic parcels of the two closely-related primate species, thus enabling region-based and network-based comparisons in revealing mechanisms in brain evolution and development.

Due to huge differences in brain size and anatomical structure (e.g., cortical folding patterns) across species and age (Fig. 1), conventional anatomical landmarks based parcellations are not suitable for defining the joint parcellation maps. Considering the dynamic development of both human and macaque infant brains, it is more meaningful to create joint cortical parcellation maps based on the developmental pattern of cortical properties (e.g., surface area). This is because the dynamic developmental patterns of cortical properties in both human and macaque infant brains implicitly reflect the underlying changes of their cortical microstructures (e.g., dendritic and synaptic architecture), which essentially determine the molecular and functional principles of the cerebral cortex [2]. Hence, developmental patterns of cortical properties during infancy are well suitable for defining distinct cortical regions in structures and functions. However, we still lack methods for joint parcellation of human and macaque infant cortical surfaces.

To address this issue, we propose a novel method to jointly parcellate human and macaque infant cortical surfaces based on their developmental patterns of cortical surface area. Indeed, there is a remarkable similarity of cortical surface areal expansion patterns between brain development and evolution [4]. To comprehensively characterize developmental patterns of cortical vertices, we define two feature vectors at each vertex, i.e., 1) growth trajectory and 2) growth correlation profile. Based on these two features, we construct two similarity matrices for each species. To effectively leverage both common and complementary information of human and macaque infants, we hierarchically non-linearly fuse these four similarity matrices into a single matrix for joint parcellation using spectral clustering [6]. Based on 210 longitudinal MRI scans of 36 human infants and 140 longitudinal MRI scans of 30 macaque infants, we create the *first* biologically-meaningful joint parcellation maps of human and macaque infants.

2. METHOD

2.1. Datasets and Cortical Surface Mapping

Longitudinal T1w and T2w human brain MRI scans were acquired from 36 normal infants (18 males) during the first two postnatal years. Each infant has 4 to 7 longitudinal scans using a Siemens 3T scanner, with the imaging acquisition parameters as in [7]. Longitudinal T1w and T2w macaque brain MRI scans were from a public neurodevelopment dataset with 30 infant rhesus macaques (15 males) from 0 to 24 months [8]. Each macaque has 4 to 5 longitudinal scans with acquisition parameters detailed in [8].

Each T2w image was rigidly aligned onto the corresponding T1w image and further resampled to be isotropic. Skull stripping and tissue segmentation were performed using a learning-based method [9]. Cortical surfaces were reconstructed and mapped onto a spherical space following an infant-specific pipeline [7]. To establish intra-subject cortical correspondences, all longitudinal spherical surfaces were group-wisely aligned and the intra-subject mean cortical folding map was generated [10]. To define within-species inter-subject cortical correspondences, intra-subject mean cortical folding maps of all subjects were group-wisely aligned and then two within-species mean cortical folding maps were generated accordingly. To further establish inter-species (human-macaque) correspondences, these two within-species mean cortical folding maps were further respectively aligned onto PALS-B12 human atlas and F99 macaque atlas, where inter-species correspondences were established using 23 functional landmarks [11]. Finally, each surface was resampled based on the alignment and the cortical properties (e.g., surface area, cortical thickness, and sulcal depth) were computed for each vertex.

2.2. Construction of Similarity Matrices of Cortical Developmental Patterns

We adopt surface area as an example for constructing cortical developmental patterns, since surface area expands more rapidly during infancy compared to other cortical properties. To comprehensively characterize the developmental patterns, for each vertex i of each subject n, we first defined two feature vectors, i.e., 1) growth trajectory of surface area $\boldsymbol{F}_1^n(i)$ and 2) growth correlation profile of surface area $\boldsymbol{F}_2^n(i)$. Specifically, for each vertex, its growth correlation profile was defined as the Pearson's correlation coefficient between its growth trajectory of surface area and that of each of the 160 reference points uniformly sampled on the cortical surface. Using these two feature vectors $\boldsymbol{F}_1^n$ and $\boldsymbol{F}_2^n$, we constructed two complementary subject-specific similarity matrices $\boldsymbol{S}_1^n$ and $\boldsymbol{S}_2^n$, respectively.

Specifically, for each subject, between each pair of vertices i and j, we computed the Pearson's correlation coefficient $p(\cdot,\cdot)$ of their feature vectors, thus obtaining their subject-specific similarity $\boldsymbol{S}_m^n$, $m \in \{1, 2\}$, as:

$$\boldsymbol{S}_m^n(i,j) = \frac{1 + p\left(\boldsymbol{F}_m^n(i), \boldsymbol{F}_m^n(j)\right)}{2}, i, j \in N, \quad (1)$$

where N was the total number of vertices on the cortical surface. Intuitively, in both similarity matrices $\boldsymbol{S}_1^n$ and $\boldsymbol{S}_2^n$, high correlations of feature vectors indicate high similarities of developmental patterns. Of note, as each subject had a different number and temporal distribution of time points, owing to missing scans or subject dropout, the subject-specific similarity matrices naturally solved this issue. The similarity matrix $\boldsymbol{S}_1^n$ captured the "low-order" similarity of developmental patterns. Complementarily, the similarity matrix $\boldsymbol{S}_2^n$, which is based on correlations of "correlations", captured more complex "high-order" similarity of developmental patterns. To generate population-level similarity matrices, in

each species, we averaged the low-order similarity matrices across all subjects, and also did similarly for the high-order similarity matrices. Thus, we obtained the population-level *low-order* similarity matrices, $\boldsymbol{S}_1^{\mathrm{H}}$ for human infants and $\boldsymbol{S}_1^{\mathrm{M}}$ for macaque infants, as well as the population-level *high-order* similarity matrices, $\boldsymbol{S}_2^{\mathrm{H}}$ for human infants and $\boldsymbol{S}_2^{\mathrm{M}}$ for macaque infants.

2.3. Joint Parcellation by Fusion of Similarity Matrices

Based on four complementary similarity matrices $\boldsymbol{S}_1^{\mathrm{H}}$, $\boldsymbol{S}_1^{\mathrm{M}}$, $\boldsymbol{S}_2^{\mathrm{H}}$ and $\boldsymbol{S}_2^{\mathrm{M}}$, one intuitive method to generate the joint cortical parcellation maps of the human and macaque infants is to first simply average them and then perform clustering based on the averaged matrix. However, this method cannot fully capture common and complementary information of these four matrices, thus leading to less meaningful results. To address this issue, we *hierarchically non-linearly* fused these four similarity matrices together as a single matrix $\boldsymbol{S}$. The central idea of this similarity matrix fusion strategy was to iteratively update every matrix by diffusing reliable information across matrices, thus making them more similar to each other until convergence [12]. In particular, to fuse two similarity matrices $\boldsymbol{X}_1$ and $\boldsymbol{X}_2$ into a single matrix $\boldsymbol{X}$ (where $\boldsymbol{X}_1$ and $\boldsymbol{X}_2$ represent the matrices to be fused, e.g., $\boldsymbol{S}_1^{\mathrm{H}}$, $\boldsymbol{S}_1^{\mathrm{M}}$, $\boldsymbol{S}_2^{\mathrm{H}}$ or $\boldsymbol{S}_2^{\mathrm{M}}$), for each $\boldsymbol{X}_m$, $m \in \{1, 2\}$, we computed a *full kernel* matrix $\boldsymbol{P}_m$ and *a sparse kernel* matrix $\boldsymbol{Q}_m$ as:

$$\boldsymbol{P}_m(i,j) = \begin{cases} \dfrac{\boldsymbol{X}_m(i,j)}{2\sum_{k \neq i} \boldsymbol{X}_m(i,k)}, & j \neq i \\ \dfrac{1}{2}, & j = i \end{cases}, \quad (2)$$

$$\boldsymbol{Q}_m(i,j) = \begin{cases} \dfrac{\boldsymbol{X}_m(i,j)}{\sum_{k \in N_i} \boldsymbol{X}_m(i,k)}, j \in \mathcal{N}_i \\ 0, \quad \text{otherwise} \end{cases}, m \in \{1,2\}. \quad (3)$$

Note that, $\boldsymbol{P}_1$ and $\boldsymbol{P}_2$ encoded full similarity information among all vertices, while $\boldsymbol{Q}_1$ and $\boldsymbol{Q}_2$ only captured reliable sparse high-similarity neighbors for each vertex. $\mathcal{N}_i$ represented the K nearest neighbors of vertex i in terms of similarity. At iteration t, $\boldsymbol{P}_1^{\mathrm{t}}$ and $\boldsymbol{P}_2^{\mathrm{t}}$ were then updated as: $\boldsymbol{P}_1^{\mathrm{t}} = \boldsymbol{Q}_1 \times \boldsymbol{P}_2^{\mathrm{t}-1} \times (\boldsymbol{Q}_1)^{\mathrm{T}}; \boldsymbol{P}_2^{\mathrm{t}} = \boldsymbol{Q}_2 \times \boldsymbol{P}_1^{\mathrm{t}-1} \times (\boldsymbol{Q}_2)^{\mathrm{T}}$.

Herein T indicated matrix transpose. In this way, during the iterations, the isolated weak similarities were gradually removed, while the strong similarities were preserved. Meanwhile, the weak similarities supported by both matrices were retained, depending on their neighborhood connections across these two similarity matrices. After t^* iterations, the fused matrix $\boldsymbol{X}$ was computed as the average of $\boldsymbol{P}_1^{t^*}$ and $\boldsymbol{P}_2^{t^*}$. By using this fusion method, we

first fused S_1^H and S_1^M as the joint *low-order* similarity matrix $\boldsymbol{S}_1$. Then, we fused S_2^H and S_2^M as the joint *high-order* similarity matrix $\boldsymbol{S}_2$. Next, we normalized these two joint similarity matrices $\boldsymbol{S}_1$ and $\boldsymbol{S}_2$ and further fused them as a single matrix $\boldsymbol{S}$. A last, we performed spectral clustering [6] on $\boldsymbol{S}$ to derive the joint parcellation maps of human and macaque infants. The cluster numbers were determined using both the widely-used silhouette coefficient and existing neuroscience knowledge.

3. RESULTS

3.1. Visual Inspection of Joint Parcellation Maps

Fig. 2 (a) and (b) show the parcellation results with different numbers of clusters from 2 to 15, by using the proposed fusion-based method and the simple averaging-based method, respectively. Generally, the proposed method led to biologically much more meaningful parcellations, as shown in Fig. 2 (a). Specifically, at 2-cluster parcellation, both methods identified an anterior-posterior division, separating the frontal, insula and anterior temporal regions (the anterior cluster) from the parietal, posterior temporal and occipital regions (the posterior cluster). However, when increasing the number of clusters, the proposed method revealed new clusters which tend to respect the boundaries of preceding clusters, thus indicating a meaningful *hierarchical organization* of the developmental patterning of surface area. For example, the boundaries between the frontal and parietal regions were well preserved from 2-clusters to 15-clusters by our proposed method (as indicated by black arrows). The boundaries between the dorsal prefrontal and ventral prefrontal regions appeared in 3-clusters, and were well preserved to 15-clusters by our method (as indicated by red arrows). In contrast, the corresponding boundaries by the averaging method relatively shifted across different numbers of clusters, indicating unstableness of these clusters.

3.2. Determining Cluster Numbers

To determine the appropriate numbers of clusters, we used the silhouette coefficient to evaluate our joint parcellation results. Silhouette coefficient describes the intra-cluster dissimilarity and the inter-cluster dissimilarity, computed by: $\mathrm{sc}(i) = (b(i) - a(i))/\max(a(i), b(i))$, where $\mathrm{sc}(i)$ is the silhouette coefficient for the vertex i, and $a(i)$ is the average dissimilarity between the vertex i and all other vertices in the same cluster; $b(i)$ is the minimum average dissimilarity of vertex i to any other clusters that the vertex i does not belong to. Herein, the dissimilarity between two vertices i and j is computed as $1 - \boldsymbol{S}(i, j)$. Therefore, we searched for the appropriate numbers of clusters with high and stable silhouette coefficients. Fig. 3 shows the silhouette coefficients of the joint parcellations by our method, when setting the cluster number from 2 to 18. The highest silhouette coefficient corresponds to 8-clusters. After that, the coefficient decreases and then reaches a relative stable plateau from 13-clusters to 15-clusters, and then decreases significantly after 15-clusters. To capture both the relatively coarse- and fine-scaled parcellations of developmental patterns, we adopted parcellations of 8-clusters and 15-clusters as our final results. As shown in Fig. 4, all clusters largely correspond to structurally and functionally meaningful specializations, with their approximated names shown in columns below the parcellation results.

To further verify our parcellation, we performed seed-based analyses [13] at 15 clusters for inspecting the correlation patterns of growth trajectories of surface areas of human and macaque, respectively. Herein, we used 16 relatively uniformly distributed seeds on the human and macaque infant cortical surfaces, respectively, as indicated by the centers of small surfaces in Fig. 5. In each species, the correlations between seeds and other vertices in the same cluster are always high, while the correlations between seeds and vertices in different clusters are always low. Moreover, seeds across the boundaries of clusters led to quite different patterns, indicating the meaningfulness of our parcellation.

4. CONCLUSION

This paper has two key contributions. First, we proposed a novel method for joint parcellation of human and macaque infant cortical surfaces based on their developmental patterns of cortical properties. For each species, we constructed two similarity matrices to comprehensively capture both low-order and high-order similarities of developmental patterns of vertices. To effectively leverage the information of human and macaque, we hierarchically non-linearly fused the four similarity matrices into a single matrix. Second, by applying our method, we charted the *first* development-based joint cortical parcellation maps of human and macaque infants.

Acknowledgments

This work was partially supported by NIH grants (MH107815, MH108914, MH109773, MH116225, and MH117943) and National Natural Science Foundation of China grant (U1504606).

5. REFERENCES

[1]. Rilling JK, “Comparative primate neuroimaging: insights into human brain evolution,” Trends Cogn. Sci, vol. 18, pp. 46–55, 2014. [PubMed: 24501779]

[2]. Scott JA, et al., “Longitudinal analysis of the developing rhesus monkey brain using magnetic resonance imaging: birth to adulthood,” Brain Struct. Func, vol. 221, pp. 2847–2871, 2016.

[3]. Li G, Nie J, Wang L, et al., “Mapping region-specific longitudinal cortical surface expansion from birth to 2 years of age,” Cereb. Cortex, vol. 23, pp. 2724–2733, 2012. [PubMed: 22923087]

[4]. Hill J, Inder T, Neil J, et al., “Similar patterns of cortical expansion during human development and evolution,” Proc. Natl. Acad. Sci, vol. 107, pp. 13135–13140, 2010. [PubMed: 20624964]

[5]. Van Essen DC, “Cartography and connectomes,” Neuron, vol. 80, pp. 775–790, 2013. [PubMed: 24183027]

[6]. Ng AY, Jordan MI, and Weiss Y, “On spectral clustering: Analysis and an algorithm,” Adv. Neur. In, 2002, pp. 849–856.

[7]. Li G, Wang L, Shi F, et al., “Construction of 4D high-definition cortical surface atlases of infants: Methods and applications,” Med. Image Anal, vol. 25, pp. 22–36, 2015. [PubMed: 25980388]

[8]. Young JT, et al., “The UNC-Wisconsin rhesus macaque neurodevelopment database: A structural MRI and DTI database of early postnatal development,” Front. Neurosci, vol. 11, pp. 29, 2017. [PubMed: 28210206]

[9]. Wang L, Gao Y, Shi F, et al., “LINKS: Learning-based multi-source IntegratioN frameworK for Segmentation of infant brain images,” NeuroImage, vol. 108, pp. 160–172, 2015. [PubMed: 25541188]

[10]. Yeo BT, Sabuncu MR, Vercauteren T, et al., “Spherical demons: fast diffeomorphic landmark-free surface registration,” IEEE Trans. Med. Imag, vol. 29, pp. 650–668, 2010.

[11]. Orban GA, Van Essen D, and Vanduffel W, “Comparative mapping of higher visual areas in monkeys and humans,” Trends Cogn. Sci, vol. 8, pp. 315–324, 2004. [PubMed: 15242691]

[12]. Wang B, et al., “Similarity network fusion for aggregating data types on a genomic scale,” Nat. Methods, vol. 11, pp. 333–337, 2014. [PubMed: 24464287]

[13]. Chen CH, et al., “Genetic topography of brain morphology,” Proc. Natl. Acad. Sci, vol. 110, pp. 17089–17094, 2013. [PubMed: 24082094]

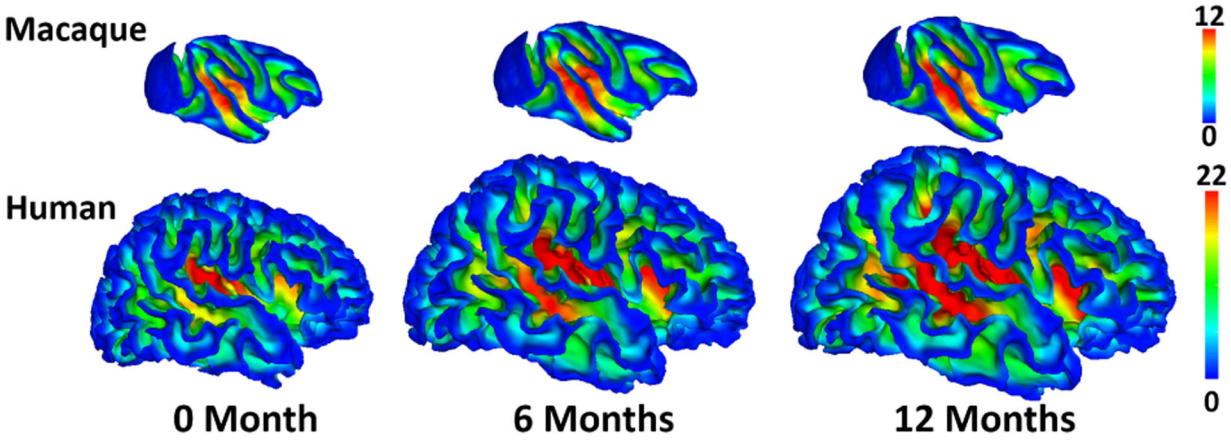

Fig. 1.

Longitudinally dynamic development of human and macaque cortical surfaces (color-coded by sulcal depth (mm)) during infancy.

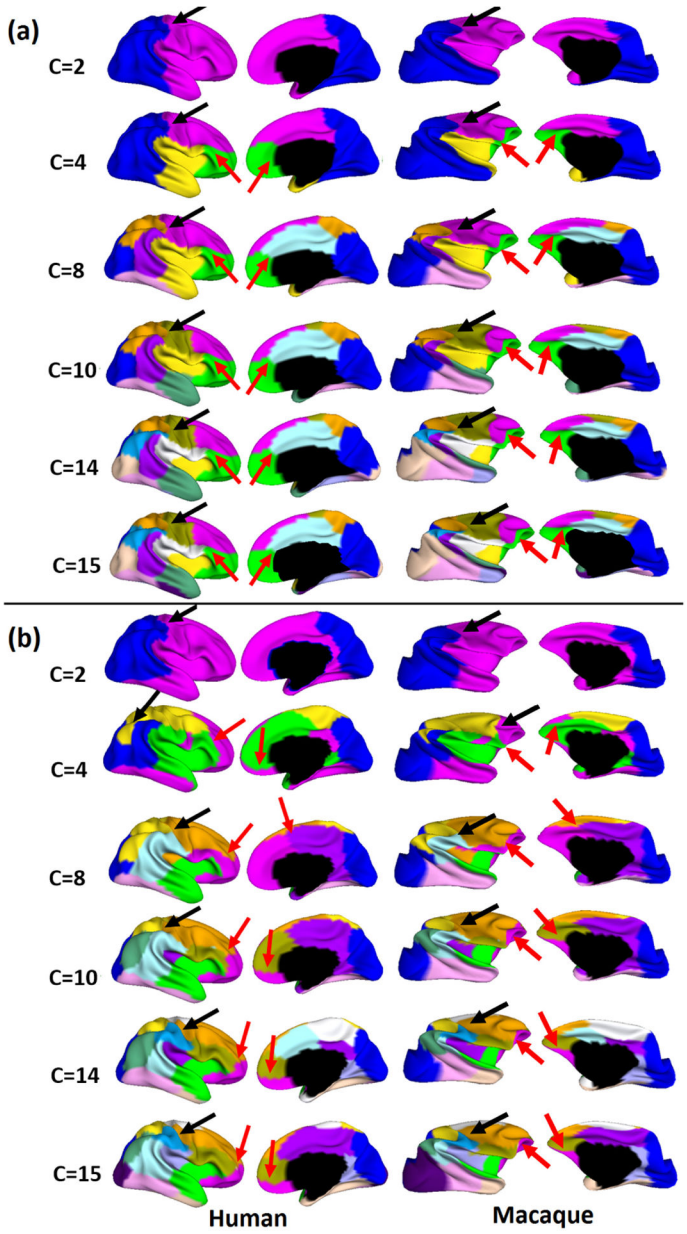

Fig. 2.

Joint cortical parcellation maps based on developmental patterns of surface areas of human and macaque infants, via (a) our proposed method by hierarchical fusion of similarity matrices and (b) a method by simply averaging all similarity matrices. C represents the number of clusters.

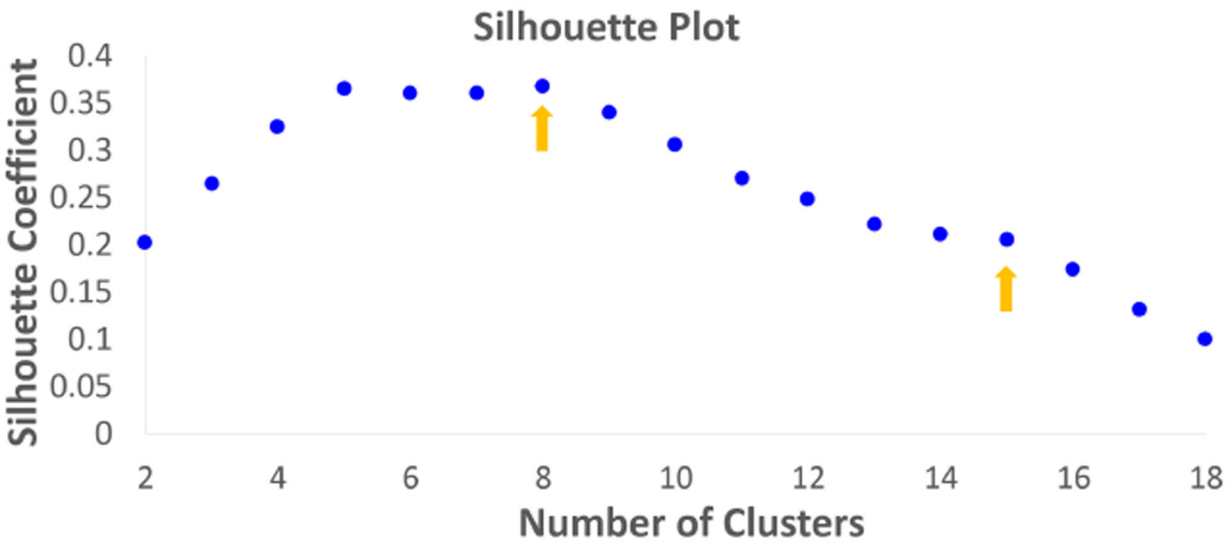

Fig. 3.
Average silhouette coefficients of the joint parcellations with different number of clusters.

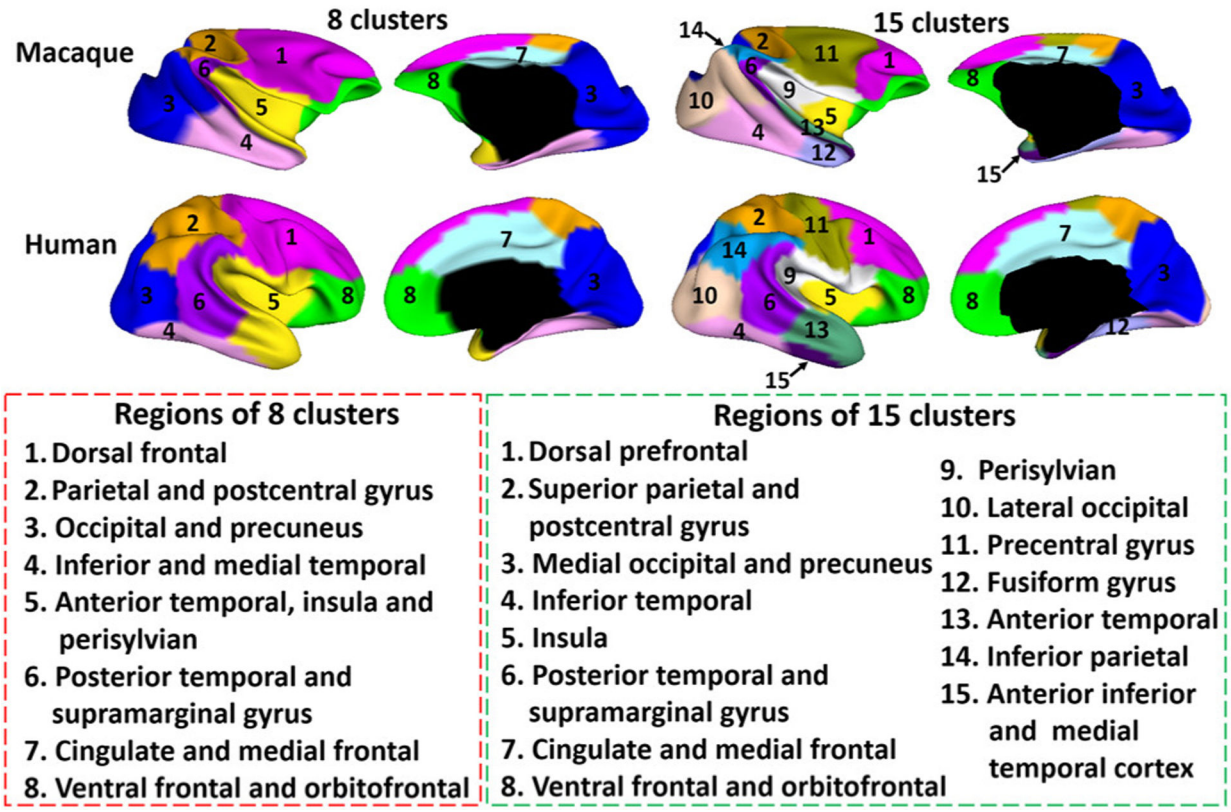

Fig. 4.
Joint parcellation results with 8-clusters and 15-clusters.

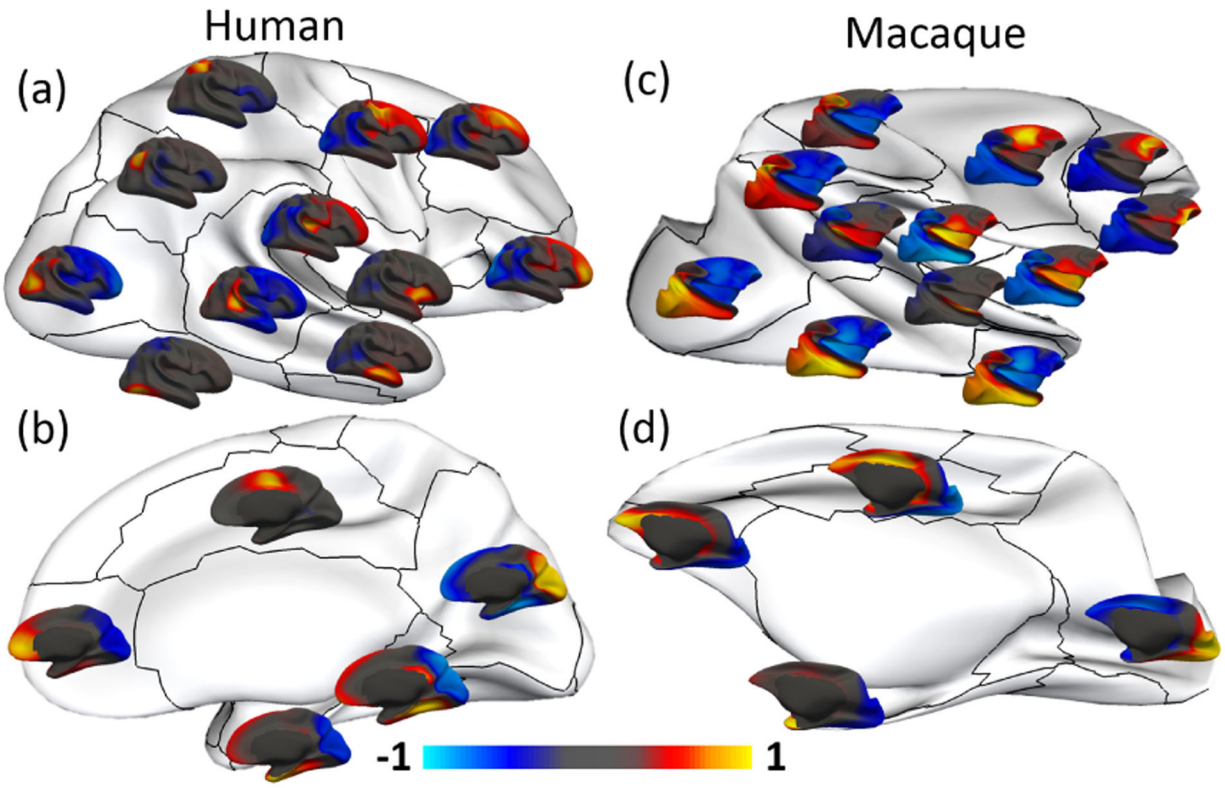

Fig. 5.

Seed-based analyses of the correlation maps of human and macaque infant developmental patterns of surface area.